Hindawi
Discrete Dynamics in Nature and Society
Volume 2021, Article ID 8011565, 17 pages
https://doi.org/10.1155/2021/8011565

Research Article

Analysis of Land Use and Land Cover Changes in Urban Areas Using Remote Sensing: Case of Blantyre City

Jane Ferah Gondwe,[1] **Sun Lin**,[1] **and Rodger Millar Munthali**[2]

[1]*College of Geomatics, Shandong University of Science and Technology, 266510 Qingdao, China*
[2]*School of Urban Construction, Yangtze University, 434000 Jingzhou, China*

Correspondence should be addressed to Jane Ferah Gondwe; jgondwe1919@gmail.com

Received 1 July 2021; Revised 6 November 2021; Accepted 3 December 2021; Published 23 December 2021

Academic Editor: Li Li

Blantyre City has experienced a wide range of changes in land use and land cover (LULC). This study used Remote Sensing (RS) to detect and quantify LULC changes that occurred in the city throughout a twenty-year study period, using Landsat 7 Enhanced Thematic Mapper (ETM+) images from 1999 and 2010 and Landsat 8 Operational Land Imager (OLI) images from 2019. A supervised classification method using an Artificial Neural Network (ANN) was used to classify and map LULC types. The kappa coefficient and the overall accuracy were used to ascertain the classification accuracy. Using the classified images, a post-classification comparison approach was used to detect LULC changes between 1999 and 2019. The study revealed that built-up land and agricultural land increased in their respective areas by 28.54 km^2 (194.81%) and 35.80 km^2 (27.16%) with corresponding annual change rates of 1.43 $km{\cdot}year^{-1}$ and 1.79 $km{\cdot}year^{-1}$. The area of bare land, forest land, herbaceous land, and waterbody, respectively, decreased by 0.05%, 90.52%, 71.67%, and 6.90%. The LULC changes in the study area were attributed to urbanization, population growth, social-economic growth, and climate change. The findings of this study provide information on the changes in LULC and driving factors, which Blantyre City authorities can utilize to develop sustainable development plans.

1. Introduction

Most parts of countries in the world are currently experiencing wide-ranging changes in land use and land cover (LULC) [1–3]. These LULC changes have mostly been associated with the interaction between humans and the environment [3–5]. The resulting negative impacts on ecosystems and human wellbeing, which include erosion, increased run-off, flooding, loss of water resources, degrading water quality, and other negative impacts, have brought these changes to the attention of the world [6–8]. There are many indicators for understanding the relation between humans and the environment, one of which is land cover change [6]. The timely and accurate understanding and monitoring of land use and land cover changes, their intensity, direction, causes, and consequences are critical for sustainable development planning; hence, it is an essential goal in the field of land cover change science [6, 9, 10].

Land cover and land use are two different terms that are frequently used interchangeably to describe land surface features [11, 12]. Land use is evidence of land utilization by humans and their habitat, mostly with an emphasis on providing information on socioeconomic activities [11], while land cover is described as the biophysical features of the Earth's surface, which includes vegetation, waterbodies, soil, and other physical features of the land [8, 13, 14]. These definitions make it clear that there is a link between land use and land cover. LULC change is a process that occurs as a result of human interaction with the physical environment, resulting in the modification and biophysical attribute change of the Earth's terrestrial surface [8, 12], by either shifting to a new type of land use or intensifying use of the existing type [12, 15]. Unfortunately, this process has negative impacts on the environment, which must be addressed if we are to achieve sustainable development [6, 9]. Changes in land use, for example, can cause

climate change, such as higher temperatures and the destruction of waterbodies, resulting in a reduction or irregular vegetation pattern, which undermines the stability of the ecosystem [16].

Rapid population growth and economic development are some of the contributing factors to this rapid change in LULC happening in most parts of the world [10, 17, 18]. Economic development and population growth cause changes in land use, as it adjusts to satisfy the demand for food and energy, as well as other capitals to support the growing population [18]. A better analysis of LULC change will not only result in accurate meaning but also ensure that there is greater knowledge of land use changes, which can be used by public or private organizations in the selection, planning, and utilization of natural resources and their management [19, 20] to meet the increasing demands for basic human needs and welfare while also achieving sustainable development goals. An understanding of the landscape patterns, changes, and relationships between human actions and natural phenomena will hence ensure that our current use of land does not adversely affect future generations [10, 21].

Since the 1970s, satellite Remote Sensing (RS) data has served as the foundation and source of information for the monitoring and analyzing of LULC changes [22]. It allows researchers to investigate changes in land cover in less time, at a cheaper cost, and with more precision [13, 23, 24]. To ensure the effectiveness of land cover change detection, RS is usually coupled with Geographic Information System (GIS) techniques [25]. It is however not the only method for analyzing the changes in LULC. Dynamic models are also used for determining the changes in and patterns of vegetation. Xue et al. used dynamic models to show how diffusion and nonlocal delay interact to produce vegetation patterns in semiarid environments [16], Brhane et al. used a mathematical model to investigate the effects of fire, rainfall, and competition for space on the dynamics of the savannah ecosystem [26], and Yan et al. used least-squares linear regression to investigate vegetation dynamics and their relationships to climatic change in southwestern China [27].

RS and GIS have been extensively utilized to give precise and timely geographical data of LULC and analyze changes in a study area [28]. RS images can efficiently capture land use conditions and serve as a good source of data for extracting, analyzing, and simulating current LULC information and changes. GIS provides a versatile platform for gathering, storing, presenting, and evaluating digital data required for change detection [12]. Remotely sensed data are very applicable and useful for LULC change detection studies [13]. Several researchers have used Remote Sensing to investigate LULC changes [12, 13, 28–30]. For example, Suzanchi et al. used multispectral satellite data of 1977 and 2001 to analyze changes in LULC of the National Capital Territory (NCT) of the Delhi region [31]. Gupta used RS and GIS to study the pattern of urban land use changes of Indian cities [32]. A case study in Algiers Town used Landsat images for urban change detection [33]. Bekturov analyzed LULC changes in Bishkek, Kyrgyzstan, between 1993 and 2003, using satellite images [34]. The mentioned studies show that RS and GIS are used in the detection of land use and cover at different scales.

Land cover classification, which is a Remote Sensing application, is used in identifying features such as land use by employing commonly multispectral satellite imagery [2]. Land cover classification using Remote Sensing images aims to associate each pixel in a Remote Sensing image with a predefined land cover category [35]. The classification techniques used in land cover classification can be categorized as either supervised or unsupervised, with numerous classification algorithms (classifiers) for each category [36–39]. Maximum Likelihood Classifier (MLC) is an example of a supervised classification approach, whereas the K-means algorithm is an unsupervised classification approach. Mohajane et al. used the maximum likelihood (ML) classification method to map LULC in Azrou Forest, in the Central Middle Atlas of Morocco [40]. More advanced methods, such as Artificial Neural Networks (ANN), a supervised classification approach, have received a lot of attention in land cover classification over the years [41]. The accuracy of the land cover classification process is influenced by a range of factors such as classification system, image data used, selection of training samples, preprocessing, classification, and postprocessing procedures, data collection, and validation methodology [2]. An accurate LULC classification map will result in a meaningful LULC change detection analysis since the generated maps are used to trace and quantify the change.

Change detection entails quantitatively analyzing changes in land cover classes using multitemporal datasets [10, 42]. It is described as the process of finding variations in an object's or phenomenon's state by monitoring it at several periods [43, 44]. Timely and accurate change detection of the Earth's surface characteristics is critical for laying the groundwork for understanding the linkages and interactions between human and natural events to improve resource management and use [42]. With the advancement of high spatial resolution satellite images and more advanced image processing software, LULC change detection, analysis, and monitoring have become more regular and consistent. Techniques for detecting changes have been categorized into several groups by authors over the years [45]. Lu et al. categorized the techniques into six groups, which are algebra, transformation, classification, advanced models, Geographic Information System (GIS) approaches, and visual analysis [10, 45]. The postclassification comparison technique, under classification category, is the most popular approach in change detection analysis [10, 44]. This approach requires individual categorization of multitemporal images into thematic maps; it then performs a pixel-by-pixel comparison of the classified images to detect regions of change [10]. The technique reduces the effects of atmospheric, sensor, and ambient variations across multitemporal pictures while still providing a comprehensive change information matrix.

Malawi is a landlocked southern African country surrounded by Mozambique, Tanzania, and Zambia [46]. Mzuzu, Lilongwe, Zomba, and Blantyre are Malawi's four largest cities, and Blantyre, where the study is situated, is the

country's commercial and industrial capital. According to the 2018 census, it has the highest population density of 3,334 people per square kilometer, up by 81% from 2,704 in 2008. In comparison, the population density of the capital city of Malawi, Lilongwe, stands at 2,455 people per square kilometer as per the 2018 census [46–48]. The study area has witnessed a tremendous change in LULC during the past decades due to urbanization, an increase in socioeconomic activities, and population. However, there has been little, if any, research to ascertain the classes of LULC and the extent of the LULC changes and their driving factors.

The main objective of this study is to analyze LULC changes in Blantyre City between 1999 and 2019 using Landsat 7 and 8 satellite imagery. To achieve the objective, it was necessary to (1) differentiate and classify the various LULC types, (2) accurately measure the magnitude and rate of LULC change, and (3) evaluate the main causes of LULC changes in the study area from 1999 to 2019. As alluded to earlier, this study will contribute to the literature on LULC for Blantyre City since the area has not been studied extensively and exclusively, and the findings are pivotal in establishing sustainable economic activity and urban planning.

2. Materials and Methods

2.1. Study Area. Blantyre City is the capital of Malawi's Blantyre District, which is located in the country's southern region. It is Malawi's commercial city, with the majority of the country's industrial and business offices. The City is located at −15°29′59.99″S, 35°00′0.00″E and has an area of 240 km^2. The study area has a total population of 809,397 people, according to the 2018 Malawi Population and Housing Census [47]. Blantyre City lies at an average elevation of 1039 meters above sea level that helps to moderate the tropical climate [49]. It has three seasons: rainy (December to March), cool (April to August), and hot (September to November). The average temperature in Blantyre is 20.7°C, and the city receives about 1086 millimeters of precipitation each year [49, 50]. The city is hilly, with Ndirande Hill being the highest point at 1595 meters above sea level [51].

As a commercial capital city, urbanization in Blantyre City is driven by natural increase, rural-urban migration, and reclassification [52]. Blantyre City has long had a young population, with a median age of 17, resulting in a situation where the population is always on the increase [47, 52]. Rural-urban migration has been driven by Blantyre City's several economic opportunities, which attract people to migrate to the city. According to the World Bank, Malawi's GDP increased at a rate of 3.9 percent per year between 1998 and 2013, owing primarily to the rise of the manufacturing and construction sectors [53]. These two are concentrated in major cities, and Blantyre contributed because the city's most important economic activities include retail industry, construction, food product manufacturing, transportation, textile industry, automobile sales and maintenance, and public administration, making it one of the country's largest employment centers. Figure 1 shows the location of the study area.

2.2. Data Collection

2.2.1. LULC Classification Data. Landsat 7 Enhanced Thematic Mapper (ETM+) images from 1999 and 2010 and Landsat 8 Operational Land Imager (OLI) images from 2019, with a resolution of 30 m, were utilized in this study to evaluate changes in LULC in the study region during a 20-year period from 1999 to 2019. Three cloud-free Landsat satellite scenes for Path/Row 167/71 from two types of sensors covering the study area were downloaded freely from the United States Geological Survey (USGS) website (http://earthexplorer.usgs.gov/). For easy visibility, the cloud-free imagery used in this study was captured during the dry season (September and October). The detailed characteristics of the Landsat images used in this study are presented in Table 1.

2.2.2. Climate Data. The paper also makes use of environmental data, specifically rainfall and temperature data, in discussing LULC class changes and determining the best time of year to extract images. For the years 1999 to 2019, rainfall and temperature data were freely obtained from the Malawi Department of Climate Change and Meteorological Services.

2.3. Image Processing and Analysis. The three satellite images were processed using the ENVI5.3 software package. The analysis was carried out using the data processing steps shown in Figure 2.

2.3.1. Image Preprocessing. Satellite image preprocessing is critical before image classification and change detection because it compensates for sensor, solar, atmospheric, and topographic effects [2, 54]. Radiometric and geometric correction of remotely sensed data is normally referred to as preprocessing [55, 56]. In this work, image preprocessing included many processes such as radiometric, geometric, and atmospheric correction, as well as image gap filling, subsetting, image enhancement, and selection of band combination. All data preprocessing procedures were performed using ENVI 5.3 software (Exelis Visual Information Solutions, Inc., Boulder, CO 80301 USA).

The radiometric correction tool in ENVI 5.3 was used to calibrate the satellite images of the years 1999, 2010, and 2019 to reduce radiometric errors. Radiometric calibration converts the digital number of pixels into spectral radiance values and the radiance into reflectance values [57]. To remove the influence of the atmosphere, the three satellite images were atmospherically corrected using the QUick Atmospheric Correction (QUAC) tool, one of the atmospheric correction tools in ENVI 5.3.

Gap filling was performed to correct for the missing data caused by the Scan Line Corrector (SLC) failure that happened on May 31, 2003, on Landsat 7's ETM+ instrument. SLC failure introduces line gaps on all Landsat 7 imagery retrieved from the failure date until 2013 [58, 59]. In this study, the Landsat 7 imagery acquired on September 21,

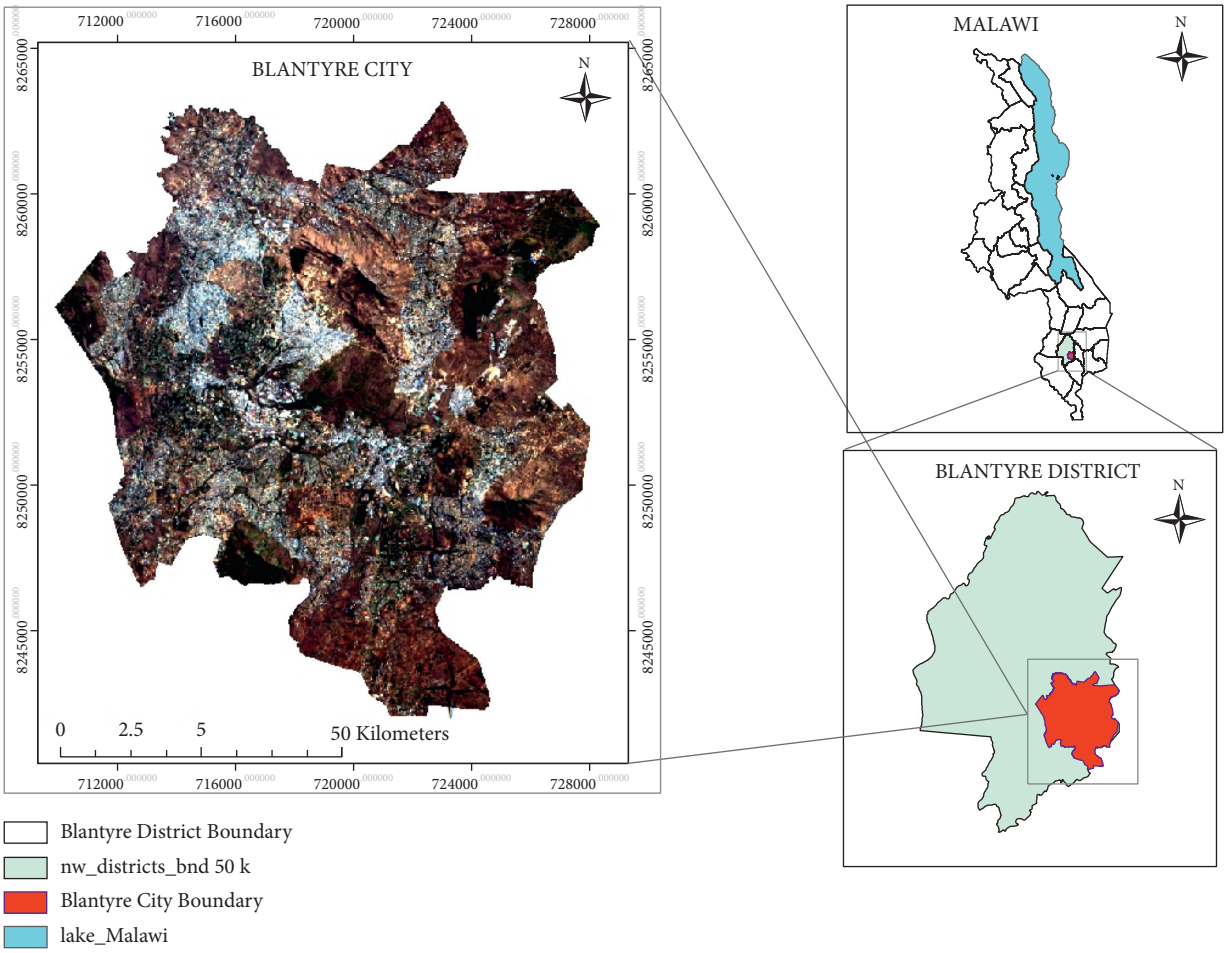

Figure 1: Location of the study area, Blantyre City. Data source: Diva GIS website and satellite image courtesy of the US Geological Survey website.

Table 1: Satellite imagery used.

Satellite sensor	Path/row	Acquisition date	Number of bands	Spatial resolution (m)
L7 ETM+	167/71	22/08/1999	8	30
L7 ETM+	167/71	21/09/2010	8	30
L8 OLI	167/71	05/08/2019	11	30

Data source: US Geological Survey.

2010, was affected by this failure. The gap-fill triangulation method in ENVI5.3 was applied to remove the gap lines and fill in the missing data. To improve the image resolution (from 30 m to 15 m), the Landsat images were sharpened using the Nearest Neighbor Diffusion (NNDiffuse). Because the downloaded satellite images' Landsat scenes spanned a considerably larger area than the study area, the image file sizes were reduced to include only the area of study by subsetting the satellite images using a shapefile specifying the study area's boundaries.

2.3.2. Image Classification. The technique of assigning a land cover classification to pixels is referred to as image classification. The procedure creates clusters of pixels with comparable digital values in the same data categories [25]. Atlas Map of Malawi Land Cover and Land Change of 1990 to 2010 prepared in 2013 by the Food and Agriculture Organization (FAO) of the United Nations [60] was used with minor modifications as a basic reference for the identification of existing LULC classes. The adopted LULC classification scheme for this study consisted of six LULC classes: built-up area, bare land, forest land, agricultural land, herbaceous land, and waterbody. Table 2 provides a description of each class.

In the present study, ANN classifier, a supervised classification approach in ENVI 5.3, was used. The theory behind supervised classification is that a user may pick sample pixels in an image that are indicative of certain classes and then instruct the image processing software to utilize these training samples as references for the categorization of all other pixels in the image. In this work, uniformly dispersed

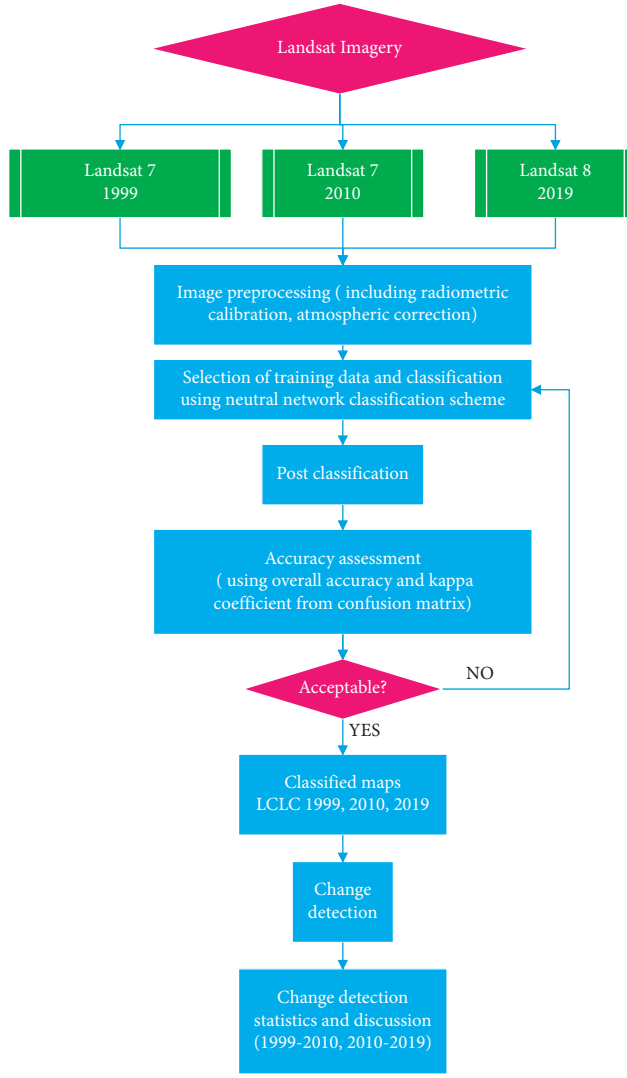

Figure 2: Flowchart of data processing steps.

Table 2: LULC class description.

LULC class	Description
Built-up land	Land that has been built on. It includes commercial, residential, industrial, and transportation infrastructure
Bare land	Areas with no dominant vegetation cover, including exposed rocks
Forest land	Areas with open woodland (15–65%), herbaceous layers, and closed broadleaved deciduous trees (>70–60%)
Herbaceous land	Including land with herbaceous closed vegetation (15–100%), permanent marsh, sparse tree, and shrub savannah
Agricultural land	Idle land being used for small-scale farming of rain-fed crops (maize) and cultivated dambo areas (BCC laws do not permit farming in the city even though small-scale farming is still practiced)
Waterbody	Areas permanently covered by water, which includes man-made dams and ponds

Regions of Interest (ROI) in the study area for all class types were identified using visual interpretation of Landsat images to train the classification. True and false composites were employed to improve the feature visualization so that LULC classes could be easily distinguished in the image. Google Earth archived images were used as references when collecting the training samples and for validating the classified maps. A total of 12690, 10362, and 11063 training samples were used for 1999, 2010, and 2019 images, respectively. A spectral separability test using the M-statistic method was performed to determine how separable the training samples were before being used in the classification. ANN algorithm, which can use backpropagation for supervised learning, was applied to generate spectral signatures and later to classify images into the above-mentioned six LULC categories.

The ANN classification is a biologically inspired computing code composed of numerous basic, highly linked processing components that imitate human brain activity to analyze information. It is considered made up of a large number of basic, linked neurons/units that function in

parallel inside a network to classify input data into output classes [61]. The input data is used to weigh the connections between the components. The weights define the amount of activation of a unit in the network, which impacts the level of activation of other units in the network and eventually dictates the network outputs [62]. The weight's magnitude is determined through an iteration procedure in which the network constantly attempts to learn the right output for each of the training samples. The procedure involves adjusting the unit weights until the Artificial Neural Network can accurately characterize the training data. To improve the results, ANN employs a set of learning rules called backpropagation (also known as backward propagation of error) [63]. This method of classification was adopted for this study due to the advantageous characteristics and capabilities it possesses, which include (1) high tolerance to noisy data, (2) the capacity to categorize patterns on which they have not been taught, and (3) the ability to incorporate various forms of data into the analysis. The ANN supervised classification method is able to perform supervised classification with less training data because the criteria for recognizing categories are based on this particular category class and other classes [64]. This method has high precision in classifying urban areas and hence its selection for this study.

The backpropagation algorithm was used in this study to train the weights and to adjust weights within a supervised classification. This type of algorithm is probably the most employed in neural network studies considering its operation. The algorithm operates under two basic steps, which are feedforward and backward. In the feedforward pass, the activation of the network flows in a single direction. This flow is from the input layer passing through the hidden layer to the output layer. The unit in a layer is connected to every unit in the next layer. However, the backward pass involves a function in which the algorithm iteratively adjusts the weights to correct the backpropagation algorithm. The network works backward from the output unit to the input units, adjusting the weight of its connections between the units so that the lowest error function between actual and desired outputs is attained [63]. Equation (1) defines the error vector, which is equal to the difference between the output and the response of the network.

$$E = \frac{1}{2} \sum (k_t - k_0)^2, \tag{1}$$

where E is the square of the error between the desired output and the real (actual) output and k_0 and k_t indicate the actual and desired output of the network, respectively.

Several training parameters were tested in this study, and the error of the ANN system's output was examined each time. Threshold training for this research study was pegged at 0.9. This was done to determine the size of the internal weight's contribution. Other types of training were done to determine the magnitude of the adjustment of the weights.

2.3.3. Postclassification. The categorized images required postprocessing to assess classification accuracy and generalize classes for output to image maps and vector GIS. A postclassification was performed to apply majority analysis to the classified map and to calculate class statistics and confusion matrices. The majority analysis reduces noise from the classified map by converting erroneous pixels within a big single class to a small class. The generated confusion matrix for each classified image was used to assess the accuracy of thematic maps.

2.3.4. Accuracy Assessment. An accuracy assessment of maps created from any remotely sensed product is a universal requirement in image classification since it allows for self-evaluation, offers a quantitative comparison of various approaches, algorithms, and analysts, and assures higher dependability of the resultant maps [65]. In this study, 85% was considered as the minimum level of interpretation accuracy in the identification of land use and land cover categories from remote sensor data according to the USGS's classification criterion [66]. In this study, an assessment of the accuracy of the classification was done using derived measures generated from the error matrix. The error matrix is the most common way to represent the classification accuracy of remotely sensed data, and it is recommended by many researchers [67]. It demonstrates the accuracy of a classification result by comparing it to the ground truth information. The error matrix reports the overall accuracy, producer and user accuracy, kappa coefficient, and errors of commission and omission. Overall accuracy, which determines the proportion of pixels that have been properly categorized, can be used to describe the overall accuracy of the map for the classes. An overall accuracy rating of greater than 70% is considered satisfactory for classification accuracy. The kappa (κ) coefficient measures the agreement between classification and ground truth pixels. In contrast to the overall accuracy, the kappa coefficient takes into account the errors of omission and commission. A kappa value of one (1) indicates perfect agreement, whereas a value of zero (0) signifies no agreement. Most applications can accept a kappa value of more than 0.75 as an excellent or very good agreement. Mathematically, the kappa coefficient (k) is presented as

$$k = \frac{N \sum_{i=1}^{n} m_{i,i} - \sum_{i=1}^{n} (G_i G_i)}{N^2 - \sum_{i=1}^{n} (G_1 G_i)}, \tag{2}$$

where i represents the class number, N is the total number of classified pixels relative to the ground truth, $m_{i,i}$ denotes the number of pixels of ground truth class i, which have also been assigned to class i, C_i is the total number of classified pixels in class i, and G_i refers to the total number of ground truth pixels in class i.

2.3.5. LULC Change Detection. The technique of identifying changes in land cover by analyzing Remote Sensing images in the same geographical area at various times is referred to as change detection [68]. In this study, LULC change detection was accomplished using a postclassification comparison technique to track LULC changes that happened

over a twenty-year period. A thematic change detection algorithm using ENVI 5.3 was applied by comparing pairs of the three produced LULC classification maps (1999, 2010, and 2019) to the produced change maps. Using the change detection statistics tool in ENVI 5.3, change matrices (a comprehensive list of the differences between each pair of classification images) were produced to assess the magnitude of change for the periods of 1999 to 2010, 2010 to 2019, and 1999 to 2019.

3. Results

3.1. Accuracy Assessment. An accuracy assessment was carried out for the three classified maps to verify if what was mapped corresponds to what exists on the ground. The classification accuracy was evaluated through the error matrix. Overall accuracy, kappa coefficient, and the user and producer's accuracy obtained from the error matrix were used to verify the accuracy of the three classified maps. For 1999, 2010, and 2019, the overall accuracies were 89.71%, 85.50%, and 87.06%, respectively, indicating that the three classified maps met the USGS's classification criterion of the overall accuracy of 85% in classifying land use and land cover classes from remote sensor data. In addition, all three classified maps achieved kappa coefficient values of 0.82, 0.78, and 0.76 in 1999, 2010, and 2019, respectively, thus greater than 0.75, indicating that the classification is significantly better. User and producer's accuracies of individual classes for each year of the land cover map are presented in the error matrix shown in Table 3.

3.2. LULC Classification Analysis. The classification of the three Landsat images resulted in a LULC map for each year, as shown in Figure 3, which depicts the distribution of the six classes in the study area. Table 4 shows the area statistical distribution of LULC and their proportions for the three years based on the classification results. The findings indicate that agricultural land is the most dominant land class in the studied area. In 1999, 2010, and 2019, the agricultural land class occupied 131.83 km^2, 170.71 km^2, and 167.63 km^2, respectively, accounting for 57.15%, 74%, and 72.67% of the total area. Herbaceous land was the second largest class in 1999 and 2010, representing 26.46% and 12.03% of the total land, respectively, while in 2019, it was the third largest class, with 7.5 percent of the total area. As regards the built-up area, the class is distributed across the research region, with a concentration in the northwest part. The built-up area occupied 6.35%, 11.76%, and 18.72% of the total land in the respective years of 1999, 2010, and 2019. Forest land occupied 9.83%, 1.97%, and 0.93% of the total area, making it the third dominating class in 1999 and the fourth largest in 2010 and 2019. The waterbody class has an area percentage of 0.13%, 0.11%, and 0.12% of the entire area over the study period. The smallest class in the study area in 1999 and 2019 is bare land, with 0.09% and 0.07% of the total area.

3.3. LULC Change Detection Analysis. The postclassification comparison change detection results show that LULC has changed greatly in the study area over the last two decades. The change matrix in Table 5 shows the amount and type of change that has occurred in each LULC class. The change matrix and statistics from 1999 to 2010, 2010 to 2019, and 1999 to 2019, which were constructed using the classified maps 1999, 2010, and 2019, and the population data of Blantyre presented in Table 6 will be used to discuss the changes that have taken place over the study period in depth in the following sections.

3.3.1. LULC Change Detection between 1999 and 2010. Agriculture was by far the most prominent LULC class type in the studied area in 1999, accounting for 57.15% of the total land, followed by herbaceous land, forest, built-up area, waterbody, and lastly, bare land, accounting for 0.09% of the total land. Between 1999 and 2010, the classes of herbaceous forests and waterbody experienced a decline in their respective areas. Table 7 provides a summary of the major changes in LULC in the study region between 1999 and 2010.

Table 7 shows that the area of the waterbody declined from 0.29 km^2 (0.13% of the total land) in 1999 to 0.26 km^2 (0.11%) in 2010, with a minimal decrease of 0.03 km^2 (10.34% of the initial area). The decrease represents a negative annual change rate of 0.94%. Table 5 shows that only 0.26 km^2 of the 0.29 km^2 waterbody remained unchanged from 1999 to 2010; however, 0.03 km^2 changed classes. During this time frame, 0.01 km^2 was converted to agricultural land, whereas 0.02 km^2 was transformed into herbaceous land.

Over the study period, there has been a significant loss of herbaceous land in the study area. In 2010, compared to 1999, the herbaceous area decreased by 33.28 km^2 (54.52% of the initial) at a negative annual rate of 3.03 $km{\cdot}year^{-1}$ (4.96%). Only 18.89 km^2 of the 61.04 km^2 herbaceous area remained unchanged in 1999, while 42.15 km^2 changed classes in 2010. A larger area of herbaceous land (40.06 km^2) was converted to agricultural land, whereas 1.85 km^2 was converted to a built-up area. The remaining 0.24 km^2 transitioned into bare land and forest land.

Between 1999 and 2010, forest land declined by 18.12 km^2 (79.93%) from 22.67 km^2 to 4.55 km^2, as shown in Table 7. Table 5 shows that 18.31 km^2 of the total area of forest land (out of 22.67 km^2) was converted to other classes in 2010, while 4.36 km^2 remained constant. Out of 18.312 km^2 of forest land that changed classes, more than half changed into agricultural land (10.78 km^2), while 7 km^2 changed into herbaceous land and 0.52 km^2 was converted to the built-up area. The smallest transition was to bare land, registering 0.01 km^2.

The class of bare land is the least dominant in the year 1999, accounting for only 0.09% of the total area. During this period, the area of bare land increased from 0.20 km^2 in 1999 to 0.27 km^2 in 2010, representing a 0.07 km^2 increase (35% of the initial area) and a 0.01 $km{\cdot}year^{1}$ annual growth rate. Table 5 shows that, between 1999 and 2010, 0.03 km^2 of bare land remained unchanged in 2010, while a total of 0.17 km^2 changed classes. The largest transition was to agricultural land with 0.16 km^2.

Table 3: Error matrix: accuracy assessment for land cover maps of 1999, 2010, and 2019.

LULC class	Built-up area	Forest land	Bare land	Herbaceous land	Agricultural land	Waterbody	Row total	Producer's accuracy (%)
				1999				
Built-up area	402	1	0	6	37	0	446	90.13
Forest land	0	7710	0	256	62	2	8030	96.01
Bare land	0	0	215	1	3	0	219	98.17
Herbaceous land	12	363	65	1512	138	0	2090	72.34
Agricultural land	11	197	11	122	1254	0	1595	78.62
Waterbody	0	17	0	0	2	291	310	93.87
Column total	425	8288	291	1897	1496	293	12690	
User's accuracy	94.59	93.03	73.88	79.70	83.82	99.32		
Overall accuracy (%)	89.71							
Kappa coefficient	0.82							
				2010				
Built-up area	641	0	12	0	1	0	654	98.01
Forest land	0	1564	0	52	127	11	1754	89.17
Bare land	17	0	216	0	17	0	250	86.40
Herbaceous land	1	292	0	1196	194	0	1683	71.06
Agricultural land	33	605	17	122	5020	1	5798	86.58
Waterbody	0	1	0	0	0	222	223	99.55
Column total	692	2462	245	1370	5359	234	10362	
User's accuracy	92.63	63.53	88.16	87.30	93.67	94.87		
Overall accuracy (%)	85.50							
Kappa coefficient	0.78							
				2019				
Built-up area	788	0	3	0	37	0	828	95.17
Forest land	2	888	5	163	77	0	1135	78.24
Bare land	6	0	240	0	32	0	278	86.33
Herbaceous land	1	146	5	1774	343	2	2271	78.12
Agricultural land	63	108	44	390	5661	0	6266	90.34
Waterbody	0	1	1	0	3	280	285	98.25
Column total	860	1143	298	2327	6153	282	11063	
User's accuracy	91.63	77.69	80.54	76.24	92.00	99.29		
Overall accuracy (%)	87.06							
Kappa coefficient	0.76							

During this 11-year time frame, the results in Table 7 show that the class of built-up area increased by 12.48 km^2, that is, 85.19% of the initial. The area coverage of the built-up area class increased from 14.65 km^2 (6.35% of total land) in 1999 to 27.13 km^2 (11.76%) in 2010. The change represents an increase in the built-up area with an annual change rate of 1.13 $km \cdot year^{-1}$ (7.74%). As shown in Table 5, out of 14.65 km^2 of the total built-up area in 1999, 14.15 km^2 remained unchanged in 2010, while 0.50 km^2 changed classes.

The area of agricultural land increased by 30.88 km^2 between 1999 and 2010, from 131.83 km^2 to 170.71 km^2, registering the highest annual change rate of 3.53 $km \cdot year^{-1}$. During this period, out of 131.83 km^2 of the total land in 1999, 119.35 km^2 remained unchanged in 2010, whereas 12.48 km^2 changed classes. As shown in Table 5, the transition was into the built-up area, herbaceous area, forest land, and bare land classes. The greatest change was into the built-up area (10.61 km^2), followed by the herbaceous class (1.77 km^2), and the smallest change was into bare land (0.03 km^2).

3.3.2. LULC Change Detection between 2010 and 2019. The results in Table 8 show that the forest area continued to decrease in the second period of the study. The forest area declined by 52.75%, from 4.55 km^2 in 2010 to 2.15 km^2 in 2019, with an annual change rate of −0.27 $km \cdot year^{-1}$ (4.36%). Table 5 shows that, out of 4.55 km^2 area of forest, 2.01 km^2 did not change in the subsequent nine years, while 2.54 km^2 switched classes. Most of the forest land was converted to agricultural land with 1.04 km^2, whereas 0.97 km^2 changed to herbaceous land, 0.51 km^2 to the built-up area, and 0.02 km^2 into bare land. Similarly, the class of herbaceous land also continued to decline. Its area decreased by 10.47 km^2, from 27.76 km^2 to 17.29 km^2, with an annual change rate of 1.16 $km \cdot year^{-1}$ between 2010 and 2019. During the study period, 14.87 km^2 of herbaceous land remained in the same class, whereas 12.89 km^2 changed classes. A large portion of the herbaceous area (12.76 km^2) was converted to agricultural land, whereas 0.45 km^2 was transformed to the built-up area (0.35 km^2), forest land (0.07 km^2), and bare ground (0.03 km^2). Population increase

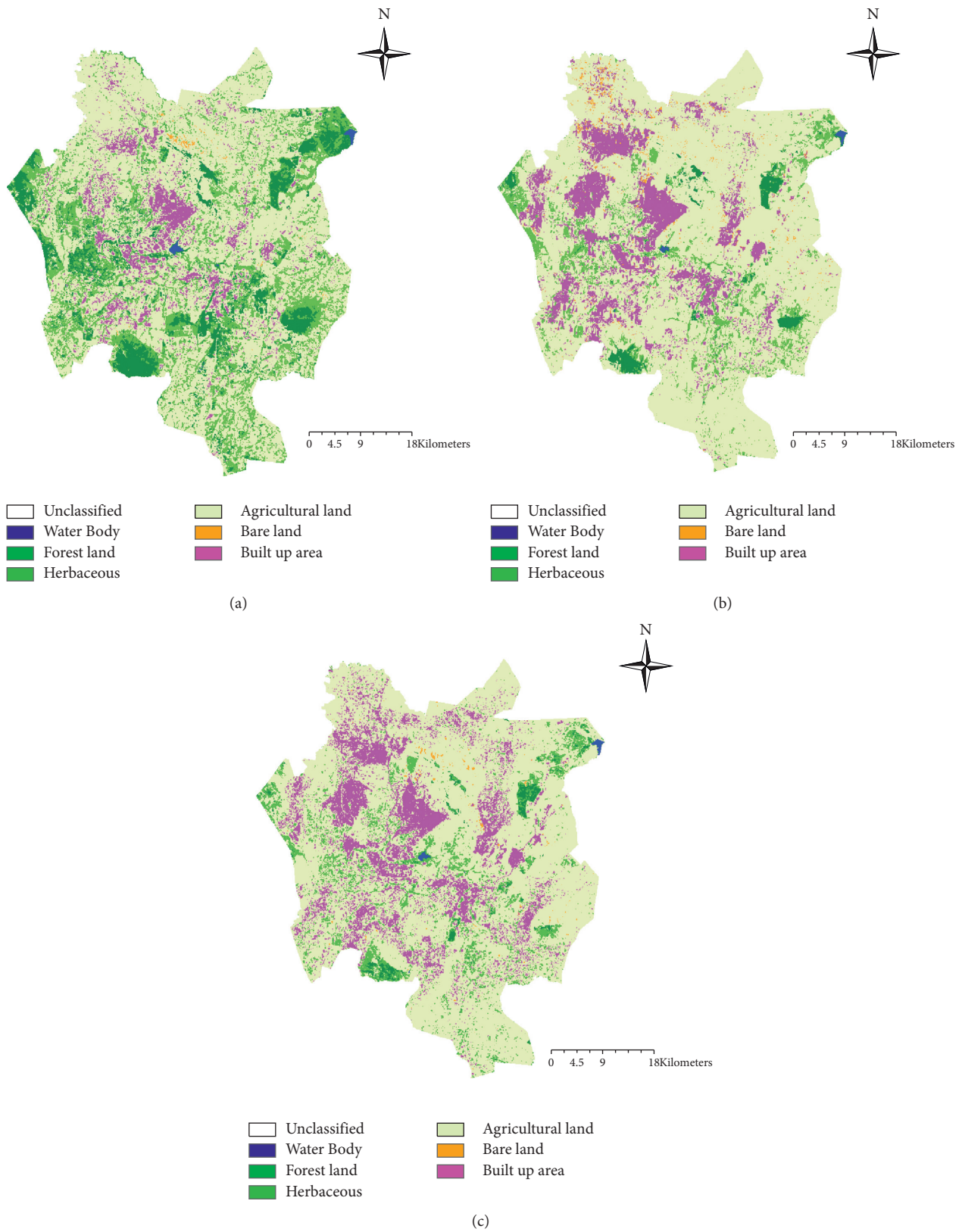

Figure 3: LULC map for (a) 1999, (b) 2010, and (c) 2019. Data source: satellite images courtesy of the US Geological Survey website.

Table 4: LULC area statistics for 1999, 2010, and 2019.

LULC classes	1999		2010		2019	
	Area (km^2)	%	Area (km^2)	%	Area (km^2)	%
Built-up area	14.65	6.35	27.13	11.76	43.19	18.72
Forest land	22.67	9.83	4.55	1.97	2.15	0.93
Bare land	0.20	0.09	0.27	0.12	0.15	0.07
Herbaceous land	61.04	26.46	27.76	12.03	17.29	7.5
Agricultural land	131.83	57.15	170.71	74.00	167.63	72.67
Waterbody	0.29	0.13	0.26	0.11	0.27	0.12
Total	230.68	100	230.68	100	230.68	100

Table 5: LULC class change/transition matrix.

	LULC class	Built-up area	Forest land	Bare land	Herbaceous land	Agricultural land	Waterbody	Class total
				1999 LULC area (km^2)				
2010 LULC	Built-up area	14.15	0.52	0.00	1.85	10.61	0.00	27.13
	Forest land	0.02	4.36	0.00	0.10	0.07	0.00	4.55
	Bare land	0.06	0.01	0.03	0.14	0.03	0.00	0.27
	Herbaceous land	0.07	7.00	0.01	18.89	1.77	0.02	27.76
	Agricultural land	0.35	10.78	0.16	40.06	119.35	0.01	170.71
	Waterbody	0.00	0.00	0.00	0.00	0.00	0.26	0.26
	Class total	14.65	22.67	0.20	61.04	131.83	0.29	230.68
	Class changes	0.50	18.31	0.17	42.15	20.48	0.03	
				2010 LULC area (km^2)				
2019 LULC	Built-up area	27.01	0.51	0.01	0.35	15.31	0.00	43.19
	Forest land	0.01	2.01	0.00	0.07	0.06	0.00	2.15
	Bare land	0.00	0.02	0.08	0.03	0.02	0.00	0.15
	Herbaceous land	0.03	0.97	0.00	14.87	1.41	0.01	17.29
	Agricultural land	0.08	1.04	0.16	12.44	153.91	0.00	167.63
	Waterbody	0.00	0.00	0.02	0.00	0.00	0.25	0.27
	Class total	27.13	4.55	0.27	27.76	170.71	0.26	230.68
	Class changes	0.12	2.54	0.19	12.89	16.80	0.01	
				1999 LULC area (km^2)				
2019 LULC	Built-up area	13.96	2.46	0.01	3.89	22.87	0.00	43.19
	Forest land	0.00	1.97	0.00	0.08	0.10	0.00	2.15
	Bare land	0.01	0.04	0.05	0.03	0.01	0.01	0.15
	Herbaceous land	0.07	3.93	0.00	9.25	4.03	0.01	17.29
	Agricultural land	0.61	14.27	0.14	47.79	104.82	0.00	167.63
	Waterbody	0.00	0.00	0.00	0.00	0.00	0.27	0.27
	Class total	14.65	22.67	0.20	61.04	131.83	0.29	230.68
	Class changes	0.69	20.70	0.15	51.79	27.01	0.02	

Table 6: Population of Blantyre City (source: NSO).

Population			Population growth (%)			Annual growth rate (%)		
1998	2008	2018	1998–2008	2008–2018	1998–2018	1998–2008	2008–2018	1998–2018
502,053	648,852	800,264	29.24	23.34	59.40	2.92	2.33	5.94

influenced the continuous loss of forest and herbaceous land. As shown in Table 6, the population of the study area increased by 23.34% during this period, with an annual growth rate of 2.33%. As shown in Table 5, the largest transition in both forest and herbaceous classes was into agricultural land and built-up area. As the population increased, so did the demand for food and shelter. As a result, the land class in Blantyre City transitioned from herbaceous land and forest land to agricultural and built areas, resulting in a decline in herbaceous and forest land.

The area of the waterbodies in the period between 2010 and 2019, compared to the previous period (1999 to 2010), increased by 0.01 km^2 (3.89%), with an annual change percentage of 0.43%, as shown in Table 8. Table 5 shows that, in 2010, 0.01 km^2 of the waterbody was converted to herbaceous land, while 0.25 km^2 remained constant in 2019.

In comparison with the previous period, the class of bare land decreased between 2010 and 2019. Table 8 shows that the area of bare land decreased by 0.12 km^2 (44.44% of the initial) during this time frame. The decline represents an annual

Table 7: LULC class annual change rate from 1999 to 2010.

LULC classes	1999	2010	1999 to 2010			
			Change		Annual change rate	
	Area (km^2)	Area (km^2)	Area (km^2)	% of initial	$km{\cdot}year^{-1}$	%
Built-up area	14.65	27.13	20.48	85.19	1.13	7.74
Forest land	22.67	4.55	−18.12	−79.93	−1.65	−7.27
Bare land	0.20	0.27	0.07	35.00	0.01	3.18
Herbaceous land	61.04	27.76	−33.28	−54.52	−3.03	−4.96
Agricultural land	131.83	170.71	30.88	29.49	3.53	2.68
Waterbody	0.29	0.26	−0.03	−10.34	0.00	−0.94
Total	230.68	230.68				

Table 8: LULC class annual change rate from 2010 to 2019.

LULC classes	2010	2019	2010 to 2019			
			Change		Annual change rate	
	Area (km^2)	Area (km^2)	Area (km^2)	% of initial	$km{\cdot}year^{-1}$	%
Built-up area	27.13	43.19	16.06	59.20	1.78	6.58
Forest land	4.55	2.15	−2.40	−52.75	−0.27	−5.86
Bare land	0.27	0.15	−0.12	−44.44	−0.01	−4.94
Herbaceous land	27.76	17.29	−10.47	−37.72	−1.16	−4.19
Agricultural land	170.71	167.63	−3.08	−1.80	−0.34	−0.20
Waterbody	0.26	0.27	0.01	3.85	0.00	0.43
Total	230.68	230.68				

change rate of $0.01\,km{\cdot}year^{-1}$ (4.94%). Table 5 shows that, of the $0.27\,km^2$ of bare land in 2010, only $0.08\,km^2$ has remained unchanged, while $0.19\,km^2$ has changed, with $0.01\,km^2$ being converted to the built-up area, $0.02\,km^2$ to water, and $0.16\,km^2$ to agricultural land. The results in Table 8 show that the class of built-up area continued to increase during this period. The built-up area increased from $27.13\,km^2$ in 2010 to $43.19\,km^2$ in 2019, representing an increase of $16.06\,km^2$, with an annual change rate of $1.78\,km{\cdot}year^{-1}$ (6.58%). As presented in Table 5, out of the total area of $27.13\,km^2$ in 2010, $27.01\,km^2$ remained unchanged, and $0.12\,km^2$ changed classes. Compared to the previous period, the built-up area in the study area increased slightly.

In the second period of the study, the area of agricultural land decreased from $170.71\,km^2$ in 2010 to $167.63\,km^2$ in 2019, indicating a $3.08\,km^2$ change. As shown in Table 8, the decline in the agricultural class represents an annual change rate of $0.34\,km{\cdot}year^{-1}$ (0.20%). It can be seen in Table 5 that $153.91\,km^2$ out of a total of $170.71\,km^2$ of the land of agricultural land remained unchanged, while $10.80\,km^2$ changed classes. With an area of $15.31\,km^2$, the built-up region took up a bigger percentage of the transition. Furthermore, $1.41\,km^2$ changed to herbaceous land, $0.06\,km^2$ to forest, and $0.02\,km^2$ to bare land.

3.3.3. LULC Change Detection between 1999 and 2019. This period reflects the overall changes that occurred in the study area over the two decades. According to Table 9, the forest land in the study area decreased by $20.52\,km^2$ (90.52%), with an annual change rate of $1.03\,km{\cdot}year^{-1}$ (4.53%). Table 5 further reveals that, in 2019, $20.70\,km^2$ of forest land out of a total of $22.67\,km^2$ was converted to other class types, while $1.97\,km^2$ remained unchanged. A large area of forest land, covering $14.27\,km^2$, was transformed into agricultural land. The other class transition was into herbaceous land ($3.93\,km^2$), built-up area ($2.46\,km^2$), and bare land ($0.04\,km^2$).

The results of the classification reveal that the class of waterbody was $0.29\,km^2$ in 1999 and $0.27\,km^2$ in 2019. As shown in Table 9, during this period (1999 to 2019), the area of the waterbody declined by $0.02\,km^2$ (6.90%) from the initial size with a 0.34% annual change rate. Out of $0.29\,km^2$ in 1999, $0.27\,km^2$ remained unchanged while $0.02\,km^2$ changed to other classes, where $0.01\,km^2$ was converted to bare land and $0.01\,km^2$ to herbaceous land by the year 2019.

As indicated in Table 9, the class of bare land declined from $0.20\,km^2$ in 1999 to $0.15\,km^2$ in 2019, achieving a total decrease of $0.05\,km^2$, representing 25% of the initial area. During this period, the annual rate of decrease was estimated at 1.25%. Results in Table 5 show that, out of $0.20\,km^2$ area of bare land in 1999, $0.05\,km^2$ area remained unchanged, whereas $0.15\,km^2$ was converted into other classifications in 2019. A total of $0.01\,km^2$ was converted to the built-up area, while $0.14\,km^2$ was converted to agricultural land.

The results in Table 9 show that, between 1999 and 2019, the area of built-up land increased by $28.54\,km^2$, which is more than 100% of the initial area. The increase represents an annual change rate of $1.43\,km{\cdot}year^{-1}$ (9.74%). From Table 5, it can be seen that built-up land of $13.96\,km^2$ out of $14.65\,km^2$ remained unchanged in 2019. On the other hand, $0.69\,km^2$ changed to other classes in 2019, of which $0.01\,km^2$ was converted to bare land, $0.07\,km^2$ to herbaceous land, and $0.61\,km^2$ to agricultural land.

Table 9: LULC class annual change rate from 1999 to 2019.

LULC classes	1999	2019	1999 to 2019			
			Change		Annual change rate	
	Area (km^2)	Area (km^2)	Area (km^2)	% of initial	$km \cdot year^{-1}$	%
Built-up area	14.65	43.19	28.54	194.81	1.43	9.74
Forest land	22.67	2.15	−20.52	−90.52	−1.03	−4.53
Bare land	0.20	0.15	−0.05	−25.00	0.00	−1.25
Herbaceous land	61.04	17.29	−43.75	−71.67	−2.19	−3.58
Agricultural land	131.83	167.63	35.80	27.16	1.79	1.36
Waterbody	0.29	0.27	−0.02	−6.90	0.00	−0.34
Total	230.68	230.68				

Table 9 shows that, between 1999 and 2019, herbaceous land decreased by 43.75 km^2, from 61.04 km^2 to 17.29 km^2, representing an annual change rate of 2.19 $km \cdot year^{-1}$ (3.58%). During the studied period, out of 61.04 km^2 of herbaceous land in 1999, only 9.25 km^2 remained unchanged, while 51 km^2 transitioned to other classes in 2019. The major shift was into agricultural land (47.79 km^2), followed by a 3.89 km^2 change to built-up land.

Over this 20 year study period, agricultural land increased in the study area. As shown in Table 9, the area of agricultural land increased from 131.83 km^2 in 1999 to 167.63 km^2 in 2019, representing an annual change rate of 1.79 $km \cdot year^{-1}$ (1.36%). Between 1999 and 2019, 27.01 km^2 of agricultural land was converted to other classifications, while 104.82 km^2 remained constant. Table 5 shows that 22.87 km^2 of agricultural land was converted to built-up land, 4.03 km^2 to herbaceous land, 0.10 km^2 to forest land, and 0.01 km^2 to bare land.

3.4. Rainfall and Temperature Data. Data obtained from the Malawi Department of Climate Change and Meteorological Services indicate that annual rainfall amounts have been fluctuating between 729.5 mm and 1454.2 mm between 1999 and 2019, as shown in Figure 4, with the highest leap being between the years 2005 and 2006 and 2010 and 2011. During the 20-year period, the highest annual rainfall was in 2010, while the lowest was in 2005 (729.5 mm).

The changes in the mean annual temperatures were insignificant, as shown in Figure 5, in which the annual variations were between 0°C and 1.6°C. The range of the maximum temperature was from 25°C to 27.1°C, while the minimum temperature ranged from 15.7°C to 16.8°C.

4. Discussion

Blantyre City has witnessed LULC changes, as evidenced by the results from the change matrix from the post-classification comparison method of change detection. The built-up area, which increased the most among the classes by 194.81% between 1999 and 2019 (Table 9), indicates that urbanization has been one of the major factors in LULC changes. This is supported by the conversion of agricultural land, forest land, herbaceous land, and bare land into a built-up area. A decline in forest land is considered one of the characteristics that are associated with the growth in the built-up area as a result of urbanization. This is consistent with the findings of Munthali et al. who, while assessing the local perception of drivers of LULC change in Dedza district, 229 km from Blantyre City, established that the built-up area increased due to the development of agricultural areas, forest land, and bare land for commercial, academic, and business purposes [69]. Outside the region, this is comparable with the findings in Wuhan, in Hubei Province, China, and in Ethiopia [14, 70, 71].

Another factor that contributed to the increase in built-up land was the lack of enforcement of the city's plans and regulations, which resulted in informal settlements. These unplanned urban sprawls take over significant parts of the city that were not initially intended for residential purposes. The expansion in the built-up area might also be attributed to the growth in population. According to the 2018 Malawi Housing and Population Census, the population of Blantyre City increased by 29.24% between 1998 and 2008 and 23.34% between 2008 and 2018, resulting in a population density increase from 2,704 in 2008 to 3,334 in 2018 [47]. As a result of this increase in population, there is a conversion of herbaceous land to built-up land to serve the increasing population's need for land for housing.

On the other hand, the social-economic growth of the population also contributed to the increase in built-up land. Building in cities becomes more affordable as the cities' social-economic condition improves. Social-economic development might have contributed to the increase in built-up area as this period was the second term of multiparty democracy (1994), which provided citizens with the opportunity to do and own businesses freely in cities and all parts of the country.

Although the economic activities in Blantyre City are attracting multitudes to migrate to the city, not enough land is being converted into built-up land leading to the population being crammed in a limited area. This is consistent with the findings from other studies in Malawi, which revealed that, between 2001 and 2010, approximately 63% of the land remained in the same land use classification [72]. This study also found that, despite the economic activities happening in the city and agricultural land being converted into mostly built-up land, agricultural land remains the largest land by area. This is mainly because Blantyre City has several hills, rendering the land area unsuitable for either residential or commercial buildings or other economic

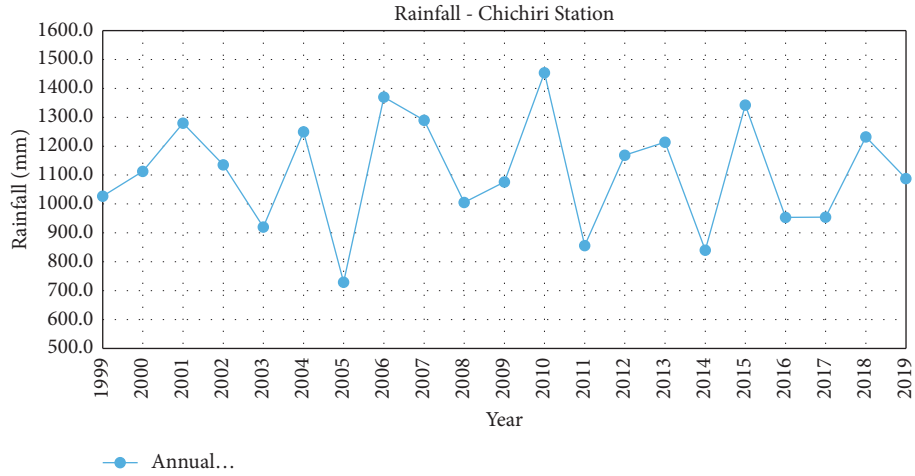

Figure 4: Total annual rainfall trends (source: Malawi Department of Climate Change and Meteorological Services).

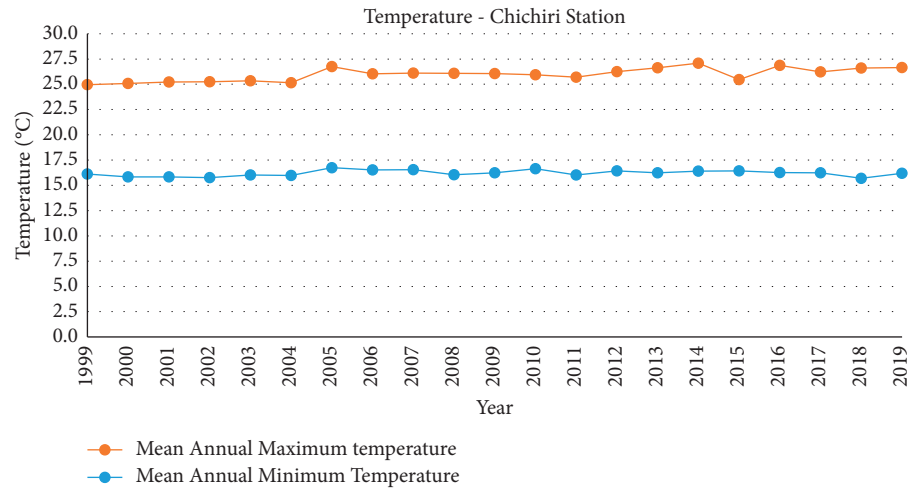

Figure 5: Maximum and minimum mean annual temperature (source: Malawi Department of Climate Change and Meteorological Services).

activities other than illicit agricultural activities. As the population grows, it becomes a challenge for city development and utility service provision to be sustainable as settlements are either sparsely distributed or densely packed. It also puts a strain on the limited amount of land available.

In the process of urbanization, the surge of people into Blantyre City has increased the demand for water in the city, resulting in reduction of waterbodies, as indicated in Table 9, which shows that the class of waterbodies has decreased by 6.9% from 1999 to 2019. The uncontrolled developments also lead to encroachment of protected catchment areas; as a result, a good amount of water is easily lost through evaporation. The decline in waterbodies is consistent with the rainfall trend in the study area, which has been inconsistent, limiting the amount of water available because most of the waterbodies in the area are artificial reservoirs. During both study periods, the study area experienced dry spells in which the annual rainfall was considerably low, and the temperatures were high. The period between 1999 and 2010 comparably received less rainfall, and during the same period, the highest maximum annual mean temperature was recorded (in 2005). This suggests that climate change is another factor that may have contributed to the decrease in the area of waterbodies.

Table 9 shows that the class of forest land has declined by 90.52%, and the class of herbaceous land has decreased by 71.67% from 1999 to 2019, indicating an overall decrease in vegetation cover. The decrease can be attributed to the encroachment of vegetation area by mainly the informal settlements being formed due to urbanization. This is, however, against the background that most of the forest areas and catchment areas for the rivers in the city are protected areas. Hence, poor enforcement of the city's plans and laws resulting in informal settlements contributed to the decrease in the area of forest and herbaceous land and eventually a reduction in area of waterbody. Climate data indicates that the study area has been experiencing occasional dry spells in which the amount of rainfall received

decreased significantly. The increased demand for timber, firewood, and modern infrastructure due to the population increase is one of the major factors that contributed to the loss of forest and herbaceous areas and consequently increase in surface temperatures. More than 97% of Malawian households use firewood and charcoal for cooking and heating [73]. Even though electricity and gas are available, they are prohibitively expensive, and power outages are common. Because alternative sources of energy are unaffordable, there is a significant increase in the demand for trees, resulting in a decline in the area of herbaceous land, forest land, and consequently waterbodies.

There is an overall increase in the agricultural area. Most of the herbaceous land was converted to agricultural land to serve the need for food for the growing population of the study area, in particular the informal settlements. Since it is difficult to monitor the progress of informal settlements in the protected areas due to poor enforcement of laws, they are also to blame for the increase in the agricultural land area because as the built-up area grows, so do informal communities that practice small-scale farming.

Limitations of this study relate to the imagery used. After Pan-sharpening, the spatial resolution of the imagery used was 15 m. An analysis of the LULC changes using satellite data with high resolution would have achieved high-quality results in that changes below the 15 m size would have been detected. Furthermore, sampling ensured that the images were cloud-free, so seasonal variations in land cover may have affected the analysis.

5. Conclusion

Remote Sensing is the most used technology in LULC change detection analysis. This study used Landsat7 ETM+ and Landsat8 OLI image data, which were downloaded and classified to detect the LULC changes in Blantyre City. ANN supervised classification was used to produce accurate LULC maps for 1999, 2010, and 2019, which were used in detecting the changes that have occurred using the postclassification comparison technique. The overall accuracy and kappa coefficient values obtained met the classification criteria. The results of the study revealed that there had been a significant change in LULC during the 20-year study period in the area. The obtained results showed that there was a decrease (from the initial area) in the area of forest land, waterbody, bare land, and herbaceous land, while the area of built-up land and agricultural land increased between 1999 and 2019. The highest increase rate of built-up land, the highest decline rate of forest land, and the highest decrease in waterbody were all achieved in the first phase (1999–2010), signifying that this was the period of great changes. The annual rate of 6.58% achieved by built-up land between the years 2010 and 2019 was only slightly lower than that recorded in the preceding period, indicating that developments are still taking place. The expansion of the built-up land was at the expense of forest land, agricultural land, and herbaceous land. The rate of decline of forest land was registered at 4.53%, with most of the land in this class converted to agricultural land between 1999 and 2010. Waterbody area declined by 0.34% in 20 years, and the largest change rate of −0.94% was registered in the first period. Thus, the observed changes indicated a decrease in the class of waterbody during the first period and an increase of 0.43% during the second period.

Several factors have been identified as contributing to the change in LULC in the study area, including population increase, social-economic growth, climate change, poor planning, and poor plan implementation. Population increase in the area influenced the increase and the decrease of built-up land and forest land, respectively. As the demand for settlement areas increased, the area of forest land decreased. The decrease in the area of forest land was due to the increase in demand for firewood, timber, and new infrastructure caused by the increased population. The decrease in the waterbody area, forest land, and herbaceous land was due to encroachment as a result of weak enforcement and application of laws and policies on the protection and conservation of the catchment areas of these waterbodies. Furthermore, environmental data has been used in discussing the changes that have occurred in land use and land cover. The data has revealed that, for a reduction in vegetation cover and waterbodies, there was a reduction in annual rainfall and an increase in the highest maximum temperature for the studied period.

The knowledge of LULC change is essential for both the land administration and land use planning activities in Blantyre City. Blantyre City Council (BCC) should consider setting aside land for nature conservation and recreational activities to mitigate the effects of climate change. It is also a recommendation of this study that the city should consider enforcing vertical development for both residential and commercial buildings to effectively use the available land. This recommendation is being made based on the fact that while the majority of the area is agricultural land, the topography is mountainous and rugged, making it unsuitable for residential development. Horizontal development is thus unsustainable because it may be required to demolish for high-rise construction in the future. These efforts should include the drafting of city-level land development plans that are compliant with current LULC and population projections. BCC should also consider developing law and policy enforcement strategies that make it difficult for developers to circumvent laws and policies while still preventing encroachment into protected areas.

Data Availability

The Landsat data used to support the findings of this study can be accessed through the following website: http://earthexplorer.usgs.gov/.

Conflicts of Interest

The authors declare no conflicts of interest.

Acknowledgments

The APC was funded by Shandong University of Science and Technology.

References

[1] J.-F. Mas, "Monitoring land-cover changes: a comparison of change detection techniques," *International Journal of Remote Sensing*, vol. 20, no. 1, pp. 139–152, 2010.

[2] J. S. Alawamy, S. K. Balasundram, A. H. M. Hanif, and C. T. B. Sung, "Detecting and analyzing land use and land cover changes in the region of Al-Jabal Al-Akhdar, Libya using time-series landsat data from 1985 to 2017," *Sustainability*, vol. 12, no. 11, p. 4490, 2020.

[3] M. Matsa, O. Mupepi, T. Musasa, and R. Defe, "A gis and remote sensing aided assessment of land use/cover changes in resettlement areas; a case of ward 32 of Mazowe district, Zimbabwe," *Journal of Environmental Management*, vol. 276, Article ID 111312, 2020.

[4] H. Briassoulis, "Factors influencing land-us and land-cover change," *Land Use, Land Cover and Soil Sciences*, vol. 1, 2011.

[5] M. Traore, M. S. Lee, A. Rasul, and A. Balew, "Assessment of land use/land cover changes and their impacts on land surface temperature in Bangui (the capital of Central African Republic)," *Environmental Challenges*, vol. 4, Article ID 100114, 2021.

[6] S. W. Wang, B. M. Gebru, M. Lamchin, R. B. Kayastha, and W.-K. Lee, "Land use and land cover change detection and prediction in the Kathmandu district of Nepal using remote sensing and gis," *Sustainability*, vol. 12, no. 9, p. 3925, 2020.

[7] H. Shiferaw, W. Bewket, T. Alamirew et al., "Implications of land use/land cover dynamics and prosopis invasion on ecosystem service values in Afar region, Ethiopia," *Science of the Total Environment*, vol. 675, pp. 354–366, 2019.

[8] E. F. Lambin, H. J. Turner, S. B. Agbola et al., "The causes of land-use and land-cover change: moving beyond the myths," *Global Environmental Change*, vol. 11, no. 4, pp. 261–269, 2001.

[9] E. M. Attua and J. B. Fisher, "Historical and future land-cover change in a municipality of Ghana," *Earth Interactions*, vol. 15, no. 9, pp. 1–26, 2011.

[10] D. Lu, P. Mausel, E. Brondízio, and E. Moran, "Change detection techniques," *International Journal of Remote Sensing*, vol. 25, no. 12, pp. 2365–2401, 2004.

[11] J. Vargo, D. Habeeb, and B. Stone Jr., "The importance of land cover change across urban-rural typologies for climate modeling," *Journal of Environmental Management*, vol. 114, pp. 243–252, 2013.

[12] C. Liping, S. Yujun, and S. Saeed, "Monitoring and predicting land use and land cover changes using remote sensing and gis techniques, a case study of a hilly area, Jiangle, China," *PLoS One*, vol. 13, no. 7, Article ID e0200493, 2018.

[13] J. S. Rawart and M. Kumar, "Monitoring land use/cover change using remote sensing and gis techniques: a case study of Hawalbagh block, district Almora, Uttarakhand, India," *The Egyptian Journal of Remote Sciencing and Space Science*, vol. 18, pp. 77–84, 2015.

[14] A. Genet, "Population growth and land use land cover change scenario in Ethiopia," *International Journal of Environmental Protection and Policy*, vol. 8, no. 4, pp. 77–85, 2020.

[15] A. W. Degife, F. Zabel, and W. Mauser, "Assessing land use and land cover changes and agricultural farmland expansions in Gambella region, Ethiopia, using landsat 5 and sentinel 2a multispectral data," *Heliyon*, vol. 4, Article ID e00919, 2018.

[16] Q. Xue, C. Liu, L. Li, G.-Q. Sun, and Z. Wang, "Interactions of diffusion and nonlocal delay give rise to vegetation patterns in semi-arid environments," *Applied Mathematics and Computation*, vol. 399, Article ID 126038, 2021.

[17] R. Wang and Y. Murayama, "Change of land use/cover in Tianjin city based on the Markov and cellular automata models," *ISPRS International Journal of Geo-Information*, vol. 6, no. 5, p. 150, 2017.

[18] S. Hussain, *Land Use/Land Cover Classification by Using Satellite Ndvi Tool for Sustainable Water and Climate Change in Southern Punjab*, COMSATS University, Islamabad, Pakistan, 2018.

[19] P. K. Mallupattu and J. R. Sreenivasula Reddy, "Analysis of land use/land cover changes using remote sensing data and GIS at an urban area, Tirupati, India," *The Scientific World Journal*, vol. 2013, Article ID 268623, 6 pages, 2013.

[20] M. Usman, R. Liedl, M. A. Shahid, and A. Abbas, "Land use/land cover classification and its change detection using multitemporal modis ndvi data," *Journal of Geographical Sciences*, vol. 25, no. 12, pp. 1479–1506, 2015.

[21] T. Kuhlman and J. Farrington, "What is sustainability?" *Sustainability*, vol. 2, no. 11, pp. 3436–3448, 2010.

[22] Y. Chang, K. Hou, X. Li, Y. Zhang, and P. Chen, "Review of land use and land cover change research progress," *IOP Conference Series: Earth and Environmental Science*, vol. 113, Article ID 012087, 2018.

[23] T. Ayala-Silv, G. Gordon, and R. Heath, "Use of satellite data to study the impact of land-cover/land-use change in Madison county Alabama," *American Journal of Applied Sciences*, vol. 6, no. 4, pp. 656–660, 2009.

[24] N. O. S. Berrick, *What Is Remote Sensing?*, NASA, Washington, DC, USA, 2021, https://earthdata.nasa.gov/learn/backgrounders/remote-sensing.

[25] P. Chaikaew, *Land Use Change Monitoring and Modelling Using Gis and Remote Sensing Data for Watershed Scale in Thailand*, IntechOpen, London, UK, 2019.

[26] K. W. Brhane, M. G. Gebru, and A. G. Ahmad, "Mathematical model for the dynamics of savanna ecosystem considering fire disturbances," *Journal of Theoretical Biology*, vol. 509, Article ID 110515, 2020.

[27] W. Yan, H. Wang, C. Jiang, S. Jin, J. Ai, and O. J. Sun, "Satellite view of vegetation dynamics and drivers over southwestern China," *Ecological Indicators*, vol. 130, 2021.

[28] A. T. Halefom, E. Sisay, D. Khare, M. Dananto, and D. T. Lakhwinder Singh, "Applications of remote sensing and gis in land use/land cover change detection: a case study of Woreta Zuria watershed, Ethiopia," *Applied Research Journal of Geographic Information System*, vol. 1, pp. 1–9, 2018.

[29] O. S. Olokeogun, F. Iyiola, and K. Iyiola, "Application of remote sensing and GIS in land use/land cover mapping and change detection in Shasha forest reserve, Nigeria," in *Proceedings of the 2014 International Archives of the Photogrammetry, Remote Sensing and Spatial Information Sciences*, Hyderabad, India, 2014.

[30] D. Pullanikkatil, L. G. Palamuleni, and T. M. Ruhiiga, "Land use/land cover change and implications for ecosystems services in the Likangala river catchment, Malawi," *Physics and Chemistry of the Earth, Parts A/B/C*, vol. 93, pp. 96–103, 2016.

[31] K. Suzanchi, R. N. Sahoo, N. Kalra, and S. Pandey, "Land use, land cover change analysis with multitemporal remote sensing data," *Multispectral, Hyperspectral, and Ultraspectral Remote Sensing Technology, Techniques, and Applications*, vol. 6405, 2006.

[32] R. Gupta, "The pattern of urban land-use changes: a case study of the Indian cities," *Environment and Urbanization ASIA*, vol. 5, no. 1, pp. 83–104, 2014.

[33] R. Bouhennache and T. Bouden, "Using landsat images for urban change detection, a case study in Algiers town," in

Proceedings of the 2014 Global Summit on Computer and Information Technology, Sousse, Tunisia, 2014.

[34] A. Bekturov, "Land use/land cover change analysis of bishkek and its impact," 2015, https://www.researchgate.net/publication/281967802_Land_use_land_cover_change_analysis_of_Bishkek_and_its_impact.

[35] X.-Y. Tong, G.-S. Xia, Q. Lu et al., "Land-cover classification with high-resolution remote sensing images using transferable deep models," *Remote Sensing of Environment*, vol. 237, Article ID 111322, 2020.

[36] K. A. Manoj, "Land cover classification from remote sensing data—geospatial world," 2010, https://www.geospatialworld.net/article/land-cover-classification-from-remote-sensing-data/.

[37] D. I. M. Enderle and J. R. C. Weih, "Integrating supervised and unsupervised classification methods to develop a more accurate land cover classification," *Journal of the Arkansas Academy of Science*, vol. 59, 2005.

[38] M. Mohammady, H. R. Moradi, H. Zeinivand, and A. J. A. M. Temme, "A comparison of supervised, unsupervised and synthetic land use classification methods in the north of Iran," *International Journal of Environmental Science and Technology*, vol. 12, no. 5, pp. 1515–1526, 2015.

[39] H. I. Mohd, H. Z. Pakhriazad, and M. F. Shahrin, "Evaluating supervised and unsupervised techniques for land cover mapping using remote sensing data," *GEOGRAFIA Online Malaysian Journal of Society and Space*, vol. 5, no. 1, pp. 1–10, 2009.

[40] M. Mohajane, A. Essahlaoui, F. Oudija et al., "Land use/land cover (LULC) using landsat data series (MSS, TM, ETM+ and OLI) in Azrou forest, in the central middle atlas of Morocco," *Environments*, vol. 5, no. 12, p. 131, 2018.

[41] S. Talukdar, P. Singha, S. Mahato et al., "Land-use land-cover classification by machine learning classifiers for satellite observations—a review," *Remote Sensing*, vol. 12, no. 7, p. 1135, 2020.

[42] H. A. Afify, "Evaluation of change detection techniques for monitoring land-cover changes: a case study in new Burg El-Arab area," *Alexandria Engineering Journal*, vol. 50, no. 2, pp. 187–195, 2011.

[43] A. Singh, "Review article digital change detection techniques using remotely-sensed data," *International Journal of Remote Sensing*, vol. 10, no. 6, pp. 989–1003, 2010.

[44] P. Deer, "Digital change detection techniques in remote sensing," 1995, http://www.dsto.defence.gov.au/corporate/reports/DSTO-TR-0169.pdf.

[45] H. Si Salah, S. E. Goldin, A. Rezgui, B. Nour El Islam, and S. Ait-Aoudia, "What is a remote sensing change detection technique? Towards a conceptual framework," *International Journal of Remote Sensing*, vol. 41, no. 5, pp. 1788–1812, 2020.

[46] UN Habitat, *Malawi: Blantyre Urban Profile*, UN Habitat, Nairobi, Kenya, 2011.

[47] Malawi Government, *2018 Malawi Housing and Population Census*, National Statistical Office (NSO), Zomba, Malawi, 2019.

[48] Government of Malawi and Ministry of Local Government, "Blantyre," 2020, https://localgovt.gov.mw/districts/181-blantyre.

[49] Britannica, "Blantyre|Malawi|britannica," 2018, https://www.britannica.com/place/Blantyre-Malawi.

[50] Meteo Climat, "Météo climat stats|station chileka/données météorologiques gratuites," 2020, http://meteo-climat-bzh.dyndns.org/index.php?page=stati&id=1546.

[51] Peakvisor, "Blantyre mountains," 2020, https://peakvisor.com/adm/blantyre.html.

[52] M. A. Z. Manda, *Malawi Situation of Urbanisation Report*, Government of Malawi, Lilongwe, Malawi, 2013.

[53] The World Bank, *Malawi Urbanization Review: Leveraging Urbanization for National Growth and Development*, The World Bank, Washington, DC, USA, 2016.

[54] N. E. Young, R. S. Anderson, S. M. Chignell, A. G. Vorster, R. Lawrence, and P. H. Evangelista, "A survival guide to landsat preprocessing," *Ecology*, vol. 98, no. 4, pp. 920–932, 2017.

[55] J. R. Jensen, *Introductory Digital Image Processing: A Remote Sensing Perspective*, Pearson Education, Inc., London, UK, 4th edition, 2015.

[56] P. V. Radhadevi, S. K. Patra, and R. Chandrakanth, "Satellite data preprocessing-new perspectives," *International Journal of Geo-Information*, vol. 4, pp. 90–98, 2003.

[57] E. A. Raabe and R. P. Stumpf, *Image Processing Methods: Procedures in Selection, Registration, Normalization and Enhancement of Satellite Imagery in Coastal Wetlands*, U.S. Geological Survey, Reston, VA, USA, 1997.

[58] F. Chen, X. Zhao, and H. Ye, "Making use of the landsat 7 SLC-off ETM+ image through different recovering approaches," in *Data Acquisition Applications. Chapter 13*Intech, London, UK, 2012.

[59] G. H. Yin, G. Mariethoz, and M. F. McCabe, "Gap-filling of landsat 7 imagery using the direct sampling method," *Remote Sensing*, vol. 9, pp. 1–20, 2017.

[60] FAO, *Atlas of Malawi Land Cover and Land Cover Changes (1990–2010)*, FAO, Rome, Italy, 2012.

[61] G. F. Hepner, T. Logan, N. Pitter, and N. Bryant, "Artificial neural network classification using a minimal training set: comparison to conventional supervised classification," *Photogrammetric Engineering and Remote Sensing*, vol. 56, pp. 469–473, 1990.

[62] G. M. Foody, M. B. McCulloch, and W. B. Yates, "Classification of remote sensed data by an artificial neural network: lssues related to training data characteristics," *Photogrammetric Engineering and Remote Sensing*, vol. 61, pp. 391–401, 1995.

[63] J. Frankenfield, *Artificial Neural Network (ANN)*, 2020.

[64] J. F. Mas and J. J. Flores, "The application of artificial neural networks to the analysis of remotely sensed data," *International Journal of Remote Sensing*, vol. 29, no. 3, pp. 617–663, 2007.

[65] A. Anand, "Accuracy Assessment," in *Processing and Classification of Remotely Sensed Images*, IGNOU, New Delhi, India, pp. 59–77, 2017, https://www.researchgate.net/3246_UNIT_14_ACCURACY_ASSESSMENT.

[66] J. R. Aderson, E. E. Hardy, J. T. Roach, and R. E. Witmer, "A land use and land cover classification system for use with remote sensor data," *Geological Survey Professional Paper*, vol. 964, 1976.

[67] R. G. Congalton, "A review of assessing the accuracy of classifications of remotely sensed data," *Remote Sensing of Environment*, vol. 37, no. 1, pp. 35–46, 1991.

[68] P. Chen, Y. Zhang, Z. Jia, J. Yang, and N. Kasabov, "Remote sensing image change detection based on nsct-hmt model and its application," *Sensors*, vol. 17, no. 6, p. 1295, 2017.

[69] M. G. Munthali, N. Davis, A. M. Adeola et al., "Local perception of drivers of land-use and land-cover change dynamics across Dedza district, central Malawi region," *Sustainability*, vol. 11, no. 3, pp. 832–925, 2019.

[70] X. Li, Y. Wang, J. Li, and B. Lei, "Physical and socioeconomic driving forces of land-use and land-cover changes: a case

study of Wuhan city, China," *Discrete Dynamics in Nature and Society*, vol. 2016, Article ID 8061069, 11 pages, 2016.

[71] E. F. Lambin and E. Geist, "Dynamics of land-use and land-cover change in tropical regions," *Annual Review of Environment and Resources*, vol. 28, no. 1, pp. 205–241, 2003.

[72] P. Jagger and C. Perez-Heydrich, "Land use and household energy dynamics in Malawi," *Environmental Research Letters*, vol. 11, no. 12, Article ID 125004, 2016.

[73] Malawi Government, *National Charcoal Strategy*, Government of Malawi, Lilongwe, Malawi, 2017.